Journal of
Ship&Ocean
Technology
©June 2000

SOTECH Vol. 4, No. 2, pp. 1 ~ 12, 2000

Application of the Weak-Scatterer Hypothesis to the Wave-Body Interaction Problems

Yonghwan Kim[1] and Paul D. Sclavounos[2]

[1] American Bureau of Shipping, Research Department, Houston, TX, USA;
E-mail: ykim@eagle.com

[2] Massachusetts Institute of Technology, Department of Ocean Engineering, Cambridge, MA, USA

Abstract

The present study concentrates on the weak-scatterer hypothesis for the nonlinear wave-body interaction problems. In this method, the free surface boundary conditions are linearized on the incoming wave profile and the exact body motion is applied. The considered problems are the diffraction problem near a circular cylinder and the ship response in oblique waves. The numerical method of solution is a Rankine panel method. The Rankine panel method of this study adopts the higher-order B spline basis function for the approximation of physical variables. A modified Euler scheme is applied for the time stepping, which has neutral stability. The computational result shows some nonlinear behaviors of disturbance waves and wave forces. Moreover, the ship response shows very close results to experimental data.

Keywords: weak-scatterer assumption, nonlinear response, Rankine panel method

1 Introduction

During last two decades, many linear and nonlinear wave-body interaction problems have been tackled. Taking the advantage of the dramatic development of computational resources, most works have adopted the numerical methods directly or indirectly. Inspired by the pioneering work of Longuett-Higgins and Cokelet(1976), many studies on the fully nonlinear wave problems have been introduced, particularly for the local wave phenomenon. However, so far, the numerical approach to the strongly nonlinear body-wave problems is limited and not matured. The nonlinear ship motion problem is a good example of such case. Because of strong interaction between body and wave, e.g. splash or slamming, it is extremely difficult to continue the stable computation when the ship motion has large amplitude. The weak-scatterer hypothesis is in the middle of the linear and fully nonlinear approaches. This hypothesis, as its name indicates, assumes the weak disturbance by a body. That is, the dominant component in total flow is the incoming flow. It should be noted that the body motion is not necessary to be small and only the disturbance by the body is assumed weak. The weak-scatterer assumption is introduced by Pawlowski(1992) from the experimental observation on the surface flow near ships in waves. In many cases, the incident wave

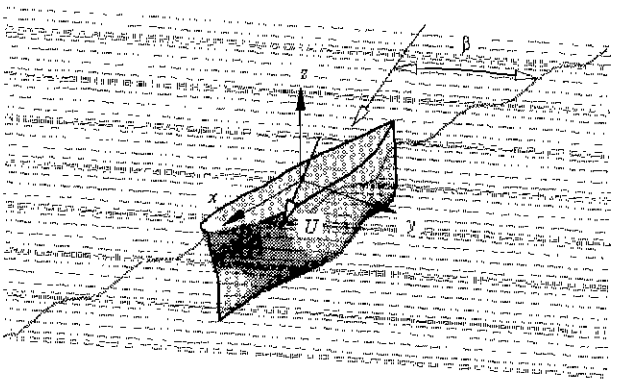

Figure 1: Coordinate system

plays a key role even though the ship experiences a large-amplitude motion. Then the scattering component can be perturbed from the incident flows, and this is the essence of the weak-scatterer assumption. Some studies, e.g. Lin and Yue(1990), have applied the Froude-Krylov force on the wetted surface by incident waves and/or the nonlinear motion of the body, combined with the linear free surface boundary condition. These studies are also based on the same idea in a large sense, but the weak-scatterer assumption takes into account higher nonlinearity. Recently, a successful application of this assumption has been reported for the ship motion in head seas(Huang and Sclavounos 1998). They showed that the weak-scatterer hypothesis predicts the transfer response functions of the heave and pitch motions closer to experimental results than the linear theory. This paper introduces the application of this hypothesis to the diffraction problem around cylinder and the ship motion in oblique sea. The diffraction problem may be a good case to observe the free surface nonlinearity which the weak-scatterer assumption can provide. In the ship motion problem, the nonlinearity of the body response will be observed.

2 Weak-Scatter Hypothesis; Formulation

Lets' define a Cartesian coordinate system, $\vec{x} = (x, y, z)$, shown in Figure 1. The coordinate origin is on the body which may move with a constant speed $\vec{U}$. The positive z-axis is oriented upwards from the still-water level. The incident waves propagate with an angle β which is defined as the angle between the negative x-axis The fluid is assumed inviscid and incompressible and flow is irrotational. Then the velocity potential of total flow $\Phi(\vec{x}, t)$, governed by the Laplace equation, can be introduced in the fluid domain.

In this study, a decomposition of the total velocity potential is introduced as follows:

$$\Psi(\vec{x}, t) = \Phi(\vec{x}, t) + \phi(\vec{x}, t) + \varphi_0(\vec{x}, t) + \varphi(\vec{x}, t) \tag{1}$$

where Φ and ϕ are the basis and local flow potentials. In addition, φ_0 and φ indicate the velocity potentials of incident wave and time-memory flow. In particular, the basis flow is the solution of the boundary value problem which applies no-flux condition on the solid boundaries and also on

the free surface defined by the given incident wave elevation. Similarly, the total wave elevation $\eta(x, y, t)$ can be decomposed into two components,

$$\eta(x, y, t) = \zeta_0(x, y, t) + \zeta(x, y, t) \tag{2}$$

where ζ_0 and ζ denote the incoming and the disturbance wave elevations, respectively.

A key assumption of the weak-scatterer hypothesis is that the basis flow, Φ, the time-local flow, ϕ, and the incident wave flow, φ_0 provide the dominant contribution to the total wave flow. that is,

$$\Phi, \phi, \varphi_0, \zeta_0 \sim O(1), \quad \varphi, \zeta \sim O(\varepsilon) \tag{3}$$

From this set of assumptions, the free surface conditions on $z = \zeta_0(x, y, t)$ can be rewritten with respect to the disturbance quantities, φ and ζ, as follows:

$$\begin{aligned}\left[\frac{\partial}{\partial t} - \left(\vec{U} - \nabla\Phi - \nabla\phi - \nabla\varphi_0\right)\cdot\nabla\right]\zeta &= -\left[\frac{\partial}{\partial t} - \left(\vec{U} - \nabla\Phi - \nabla\phi - \nabla\varphi_0\right)\cdot\nabla\right]\zeta_0 \\ &+ \frac{\partial}{\partial z}(\Phi + \phi + \varphi + \varphi_0) - \nabla\varphi\cdot\nabla\zeta_0 + \left[\frac{\partial^2\Phi}{\partial z^2} + \frac{\partial^2\varphi_0}{\partial z^2} - \nabla\left(\frac{\partial\Phi}{\partial z} + \frac{\partial\varphi_0}{\partial z}\right)\cdot\nabla\zeta_0\right]\zeta\end{aligned} \tag{4}$$

$$\begin{aligned}&\left[\frac{\partial}{\partial t} - \left(\vec{U} - \nabla\Phi - \nabla\phi - \nabla\varphi_0\right)\cdot\nabla\right]\zeta = \frac{1}{2}\nabla\varphi_0\cdot\nabla\varphi_0 \\ &- \left[\frac{\partial}{\partial t} - \left(\vec{U} - \nabla\Phi - \nabla\phi - \nabla\varphi_0\right)\cdot\nabla\right]\varphi_0 - \left[\frac{\partial}{\partial t} - (\vec{U} - \nabla\Phi)\cdot\nabla\right]\Phi + \frac{1}{2}\nabla\Phi\cdot\nabla\Phi \\ &- \left[\frac{\partial}{\partial t} - (\vec{U} - \nabla\Phi - \nabla\phi)\cdot\nabla\right]\phi + \frac{1}{2}\nabla\phi\cdot\nabla\phi - g(\zeta + \zeta_0) \\ &- \left[\frac{\partial}{\partial t} - (\vec{U} - \nabla\Phi - \nabla\phi - \nabla\varphi_0)\cdot\nabla\right]\zeta\frac{\partial}{\partial z}(\Phi + \phi + \varphi_0)\end{aligned} \tag{5}$$

During the derivation, equations (2) and (3) were applied to the exact free surface conditions and $O(\varepsilon^2)$ terms were neglected. It should be emphasized that the conditions are valid on $z = \zeta_0$.

The body boundary condition follows with the decomposition into three separate conditions for the basis, time-local, and time-memory boundary value sub-problems:

$$\frac{\partial\Phi}{\partial n} = \vec{U}\cdot\vec{n}, \quad \frac{\partial\phi}{\partial n} = \vec{\xi}\cdot\vec{n}, \quad \frac{\partial\varphi}{\partial n} = -\frac{\partial\varphi_0}{\partial n} \tag{6}$$

where $\vec{\xi}$ denotes the instantaneous body velocity vector. Note that these conditions are satisfied on the instantaneous wetted surface.

Hydrodynamic force on the body can be obtained from the integration of pressure, which is based on Bernoulli's equation as follows:

$$p = p_l + p_m + P_c \tag{7}$$

where

$$\begin{aligned} p_l = &- \rho\left[\frac{\partial}{\partial t} - (\vec{U} - \nabla\Phi - \nabla\phi - \nabla\varphi_0)\cdot\nabla\right]\phi - \frac{1}{2}\rho\nabla\phi\cdot\nabla\phi \\ p_m = &- \rho\left[\frac{\partial}{\partial t} - (\vec{U} - \nabla\Phi - \nabla\phi - \nabla\varphi_0)\cdot\nabla\right]\varphi - \rho\left[\frac{\partial}{\partial t} - (\vec{U} - \nabla\Phi - \nabla\varphi_0)\cdot\nabla\right]\varphi_0 \\ &- \frac{1}{2}\rho\nabla\phi_0\cdot\nabla\phi_0 - \rho\left[\frac{\partial}{\partial t} - (\vec{U} - \nabla\Phi)\cdot\nabla\right]\Phi - \frac{1}{2}\nabla\Phi\cdot\nabla\Phi \\ P_c = &- \rho g z \end{aligned} \tag{8}$$

The equation of body motion can be written in the form,

$$(\mathbf{M} + a_0)\ddot{\vec{\xi}} + b_0\dot{\xi} + (\mathbf{C} + c_0)\xi = \vec{F}_m(\ddot{\vec{\xi}}, \dot{\xi}, \xi, t) \tag{9}$$

where the matrix coefficients a_0, b_0, c_0 represent the time-local forces proportional to the acceleration $\ddot{\vec{\xi}}$, the velocity $\dot{\vec{\xi}}$ and the displacement $\vec{\xi}$, respectively. $\mathbf{M}$ and $\mathbf{C}$ are the mass and restoring coefficient tensors. F_m is the integrated memory force arising from surface wave effects.

3 Rankine Panel Method

The present numerical method is based on the studies of Sclavounos and Nakos(1988) for the steady flow problem and Nakos(1993) for unsteady problem. Recently, several extensions of this method are introduced by Kim et al(1997), and Huang and Sclavounos(1998).

In this method, the fluid boundary is discretized into flat panels, while the physical variables are represented with a higher-order B-spline basis function. Then, the velocity potential can be approximated as

$$\phi(\vec{x_i}, t) \approx \sum_j \phi_j(t) B_j(\vec{x_i}) = \sum_j \phi_j(t) b^{(p)}(\xi_1; \vec{x}_i) b^{(q)}(\xi_2, \vec{x}_i) \tag{10}$$

where $B_j(\vec{x}_i)$ is the B-spline basis function of order (p, q), defined on the local panel surface (ξ_1, ξ_2) and $b^{(p)}(\xi_k; \vec{x}_i)$ is the local B-spline function along ξ_k axis. The same approximation is applied to the wave elevation and normal flux on the fluid boundary.

Then, a classical boundary integral equation is obtained using Green's theorem,

$$(\varphi_k)_j^{n+1} B_{ij} + (\varphi_k)_j^{n+1} \iint_S B_{ij}(\vec{\xi}) \frac{\partial}{\partial n} G(\vec{x}; \vec{\xi}) d\xi - (\frac{\partial \varphi_k}{\partial n})_j^{n+1} \iint_S B_{ij}(\vec{\xi}) G(\vec{x}; \vec{\xi}) d\xi = 0 \tag{11}$$

where the superscript means time step, and the Green function is a simple Rankine source. Here, φ_k symbolizes all velocity potential to be involved.

The free surface conditions are integrated using a modified Euler scheme to update the disturbance wave elevations and velocity potentials on the free surface. In this scheme, the free surface elevation and velocity potential are obtained from the kinematic and dynamic conditions respectively,

$$\frac{(\zeta_k)_j^{n+1} - (\zeta_k)_j^n}{\triangle t} = P(\varphi_k^n, \zeta_k^n, \cdots\cdots) \tag{12}$$

$$\frac{(\varphi_k)_j^{n+1} - (\varphi_k)_j^n}{\triangle t} = Q(\varphi_k^n, \zeta_k^{n+1}, \cdots\cdots). \tag{13}$$

P and Q are the remaining terms in (4) and (5). Combining these with (11), the values of the velocity potentials on the submerged body surface and the normal velocities on the free surface can be obtained.

The equation of motion, (9), is numerically integrated by a fourth-order Adam-Bashford-Moulton predictor-corrector scheme. The first four time steps were integrated by a fourth-order Runge-Kutta scheme. Kring and Sclavounos(1995) showed that this method is stable as long as a set of conditions governing temporal and spatial discretization are met. Note that, in the weak-scatter formulation, the nonlinear restoring force has been included in **C**, while only the linear inertia has been considered in **M**.

An adequate implementation of the radiation condition is necessary in the truncated region of the computational domain. In the present computation, a numerical beach is employed. Over this artificial beach, the conventional method adopts a Newtonian-type cooling term, $\mu_1\zeta_k$, into the kinematic free surface condition. In this computation, an extra term, $\mu_2\varphi_k$, is added to ensure no change of the linear dispersion relation when $\mu_2 = -\mu_1^2/4g$.

4 Convergency of Numerical Method

The theoretical justification of a numerical scheme can be achieved by the stability analysis. The stability analysis for the Rankine panel method using a B-spline basis function can be found in the works of Sclavounos and Nakos for the steady wave problem(Sclavounos and Nakos 1988) and unsteady ship motion using frequency-domain approach(Nakos 1990). Moreover, Nakos and Kim et al have extended this concept to the unsteady time-domain problem (Nakos 1993, Kim et al 1997). Their analysis is limited to the linear problem, so it is not directly applicable to the weak-scatterer formulation. However, since the weak-scatterer problem recovers the nonlinear problem when the wave amplitude becomes small, it is also important to observe the numerical stability and consistency of the linear problem.

The essence of this analysis is to observe the characteristics of wave propagation in the discrete domain. The discrete dispersion relation can be obtained using the discrete Fourier transformation with respect to the space and time. When it is assumed that the panel sizes along x- and y-axes are constant, i.e. $\triangle x, \triangle y$, the triple discrete Fourier transform of the linear free surface condition and Green's identity leads to the following form of the velocity potential in the discrete domain:

$$\varphi_{l,m}^{(n)} = \frac{1}{(2\pi)^3} \iiint \frac{\widetilde{R}}{\widetilde{W}} e^{-i(ul\Delta x + vm\Delta y - wn\Delta t)} du dv dw \tag{14}$$

where the denominator, $\tilde{W}$, provides all information about wave dispersion. For the classical linear free surface boundary conditions with a forward speed U, $\tilde{W}$ takes the following form:

$$\widetilde{W} = (\beta^2 - i\beta F_h D)Z^2 - (2\beta^2 - S + F_h^2 D^2)Z + \beta^2 + i\beta F_h D \tag{15}$$

where $\beta = \sqrt{\triangle x/g\triangle t^2}$, $Z = e^{iw\triangle t}$, $F_h = U/\sqrt{g\triangle x}$, $S = \triangle x\tilde{B}/\tilde{S}_0$, $D = \tilde{D}_1/\tilde{B}$, and

$$\begin{aligned}
\widetilde{B} &= \triangle x\triangle y \sum_{m=-\infty}^{\infty}\sum_{n=-\infty}^{\infty} \frac{\sin^{p+1}(\hat{u}\pi+m\pi)\sin^{q+1}(\hat{v}\pi+n\pi)}{(\hat{u}\pi+m\pi)^{p+1}(\hat{v}\pi+n\pi)^{q+1}} \\
\widetilde{S_0} &= \frac{\triangle x^2\triangle y}{2\pi} \sum_{m=-\infty}^{\infty}\sum_{n=-\infty}^{\infty} \frac{\sin^{p+1}(\hat{u}\pi+m\pi)\sin^{q+1}(\hat{v}\pi+n\pi)}{(\hat{u}\pi+m\pi)^{p+1}(\hat{v}\pi+n\pi)^{q+1}\sqrt{(\hat{u}+m)^2+(\hat{v}+n)^2}} \\
\widetilde{D_1} &= \frac{\sum_{m=-\infty}^{\infty}\frac{\sin^{p}(\hat{u}\pi+m\pi)}{(\hat{u}\pi+m\pi)^{p}}}{\sum_{m=-\infty}^{\infty}\frac{\sin^{p+1}(\hat{u}\pi+m\pi)}{(\hat{u}\pi+m\pi)^{p+1}}}
\end{aligned} \tag{16}$$

with $\hat{u} = u\triangle x/\pi, \hat{v} = v\triangle y/\pi$.

When the panel size and time segment approach zero, we can prove that (15) becomes

$$\widetilde{W} = (w - Uu)^2 - g\sqrt{u^2+v^2} + O(\Delta x^{p+1}, \Delta t^2) \tag{17}$$

This is the continuous dispersion relation, so that the present scheme has consistency between the discrete problem and continuous problem. It is interesting that the present time stepping has the second-order accuracy even though both equation (12) and (13) have the first-order accuracy.

A condition of temporally neutral stability can be derived from (15),

$$\beta^2 - \frac{(F_h^2D^2 - S)^2}{4S} \geq 0 \tag{18}$$

5 Computational Results

5.1 *Diffraction problem around circular cylinders*

In the diffraction problem, the contribution of the weak-scatterer assumption on only the free surface nonlinearity can be observed. Figure 2 compares examples of the solution grids for the linear and weak-scatterer problems. The free surface grids for the linear problem are distributed on the still water surface and those are not necessary to be changed, while the weak-scatterer formulation requires the solution grids on the incident flow surface as well as the instantaneous wetted body surface at each time step.

Figure 3 shows the comparisons of total wave elevations between the linear and weak-scatterer solutions. In this case, the incident wave is the linear wave. The cylinder depth, d, is four times the cylinder radius, a. In addition, the wave number k is fixed but the wave amplitude A is different. When the incident wave amplitude approaches zero, the weak-scatter formulation recovers the linear formulation. As expected, the nonlinearity is more significant, particularly in local waves, when the wave amplitude is larger.

Figure 4 shows the wave profile near the cylinder when $kA = 0.10$ and $ka = 1.0$. The linear and weak-scatterer results are shown together for comparison. In this case, the incident wave is up to the second order, therefore, a part of the second-order component is already included in the weak-scatterer solution. The weak-scatterer solution shows shorter scattering wave than the linear solution which is a typical nonlinear phenomenon.

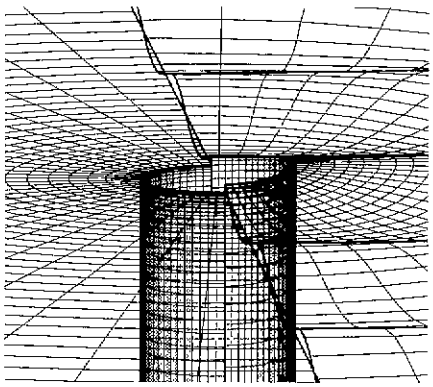

Figure 2: Comparison of solution grids; linear(left) and weak-scatter formulations(right)

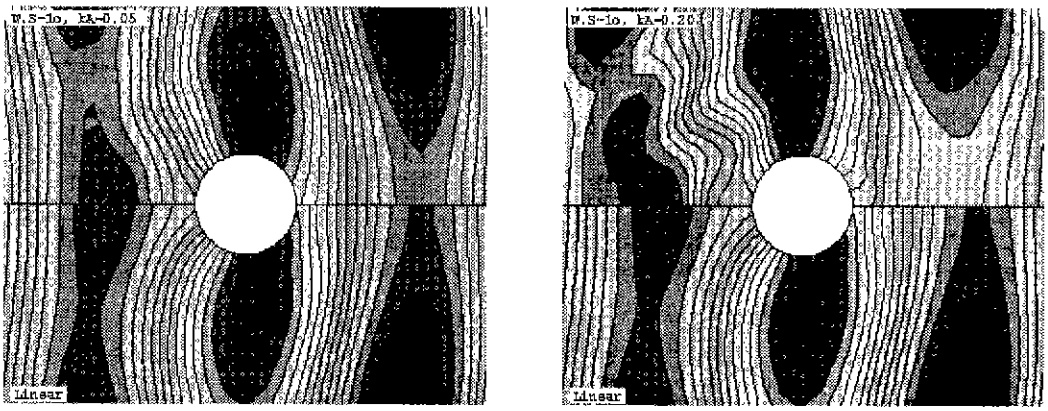

(a) $kA = 0.05$ (b) $kA = 0.20$

Figure 3: Comparison of total wave contours between linear(lower half) and weak-scatterer(upper half) solutions for two wave amplitudes; $a/d = 0.25, ka = 1.0$, W.S. indicates the weak-scatterer solution

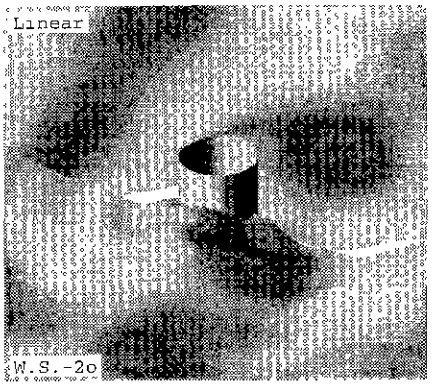

Figure 4: Comparison of wave elevations around cylinder; $ka = 1.0$, 2nd-order incident wave

Figure 5 shows the wave-induced forces on the cylinder. As the order of incident wave becomes higher, some phase shift is observed in the surge forces. A significant difference can be observed in the heave force. In particular, the double-harmonic, i.e. the second-order, component is dominant.

5.2 Nonlinear ship motions in oblique waves

S175 container ship has been considered in this study, and Figure 6 shows the solution grids at two different time steps. In the weak-scatterer formulation, the nonlinear body motion is considered, therefore the wetted hull surface as well as the free surface should be rediscretized at each time step. The hull was discretized into about 600 panels and the free surface boundary has about 1200 panels.

Figure 7 shows the time history of heave and pitch motions in the incident waves of 150^o heading. In the time-domain approach, the lateral motions cause some numerical difficulties due to no restoring force and moment, so the lateral motions were restrained in this computation. Besides, the wave amplitude A in this computation is $0.015L$ where L is the ship length. As shown in Figure 7, the ship motions becomes harmonic after several cycles.

Figure 8 shows the pressure contours on the hull surface when the wave angle is 120^o. Due to the pitch motion and hull geometry, the bow and stern areas have some pressure variations.

Figure 9 shows the three snapshots of wave contours for the different incident waves. The wave elevation of these figures includes all the components. Some reflection waves propagate downstream mixed with the steady waves, and stronger reflection can be observed at shorter incident waves. The incident wave is very dominant as shown in Figure 9(a) when the wave length is large, while the steady and diffraction wave component becomes significant at shorter waves.

Figure 10 shows the heave and pitch Response Amplitude Operators (RAOs) for 120^o heading. The RAOs are normalized with the ship length and wave number. The nonlinear effect is clear, in particular near peak, but the weak-scatterer hypothesis provides closer results to the experimental data than the strip theory. The present experimental data are from Dalzell et al(1992).

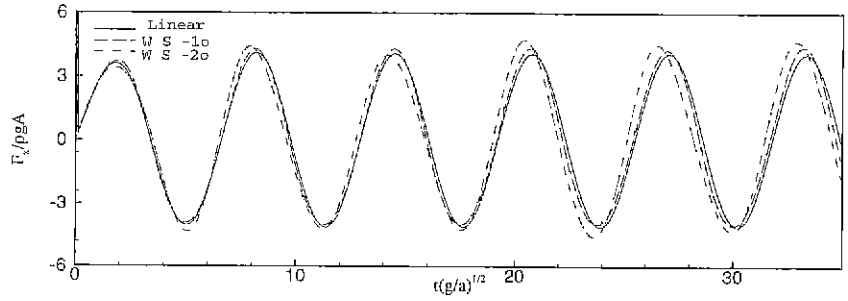

(a) $kA = 0.05$

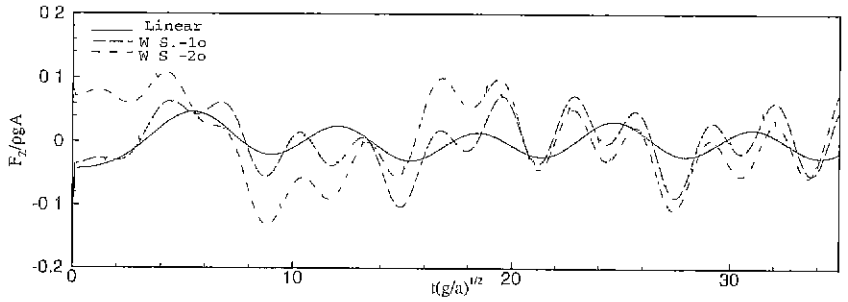

(b) $kA = 0.20$

Figure 5: Comparison of wave-induced forces; $ka = 1.0$, incident waves: W.S.-1o(linear) and W.S.-2o(2nd-order)

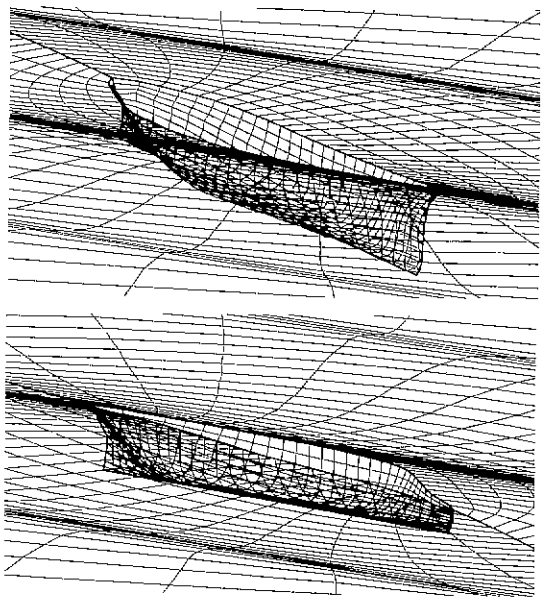

Figure 6: Two snapshots of solution grids at different time steps

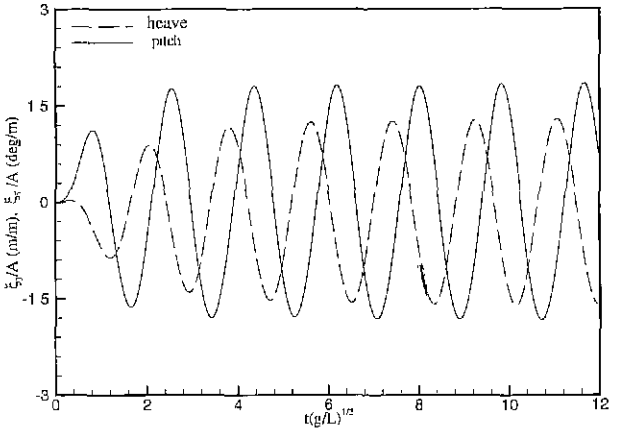

Figure 7: Time-history of the heave and pitch motions at $\omega\sqrt{L/g} = 2.25$, 150^o heading

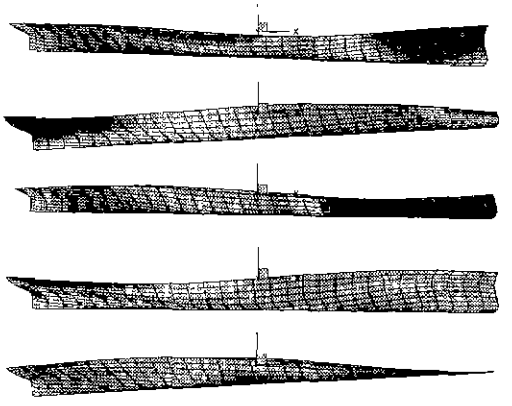

Figure 8: Pressure contour on hull surface; $\omega\sqrt{L/g} = 2.5$, 150^o heading

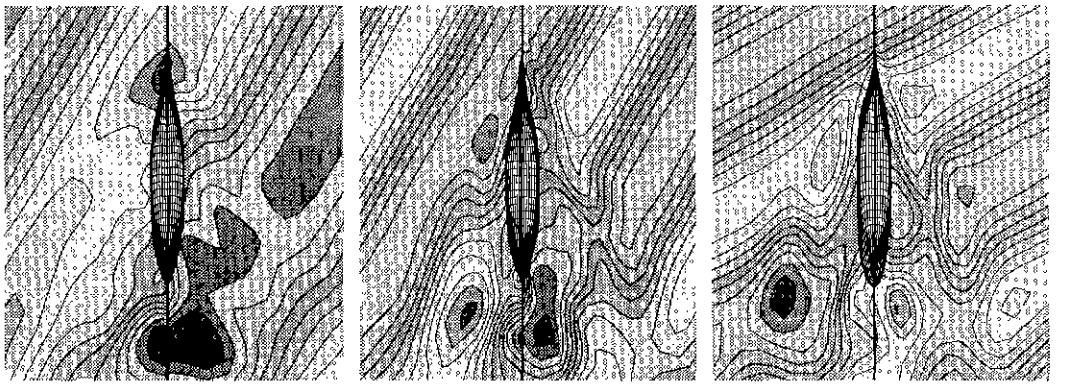

(a) $\omega\sqrt{L/g} = 2.0, 120^o$ (b) $\omega\sqrt{L/g} = 2.75, 120^o$ (c) $\omega\sqrt{L/g} = 2.5, 150^o$

Figure 9: Instantaneous elevation contours at three different wave conditions

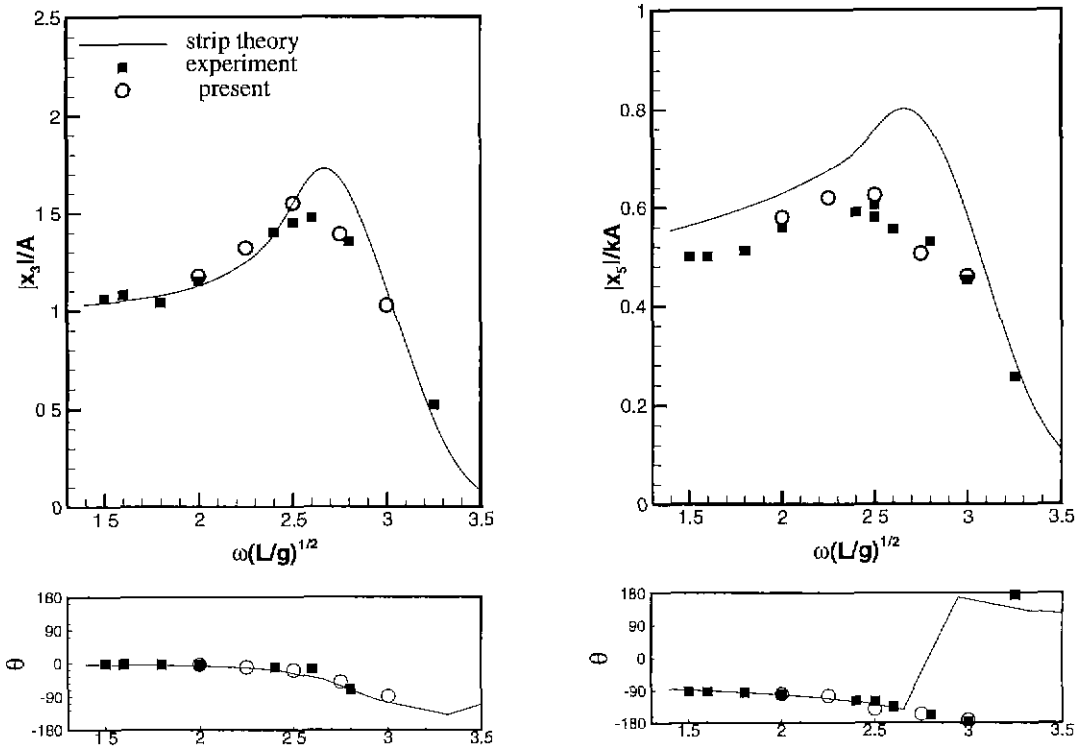

Figure 10: Heave and pitch motion RAOs; 120^o heading

6 Summary

The weak-scatterer hypothesis and its application have been introduced in this study. The weak-scatterer method assumes that the disturbance by the body motion is small compared with the incident flow. Therefore, the free surface boundary conditions are linearized on the incident wave surface. In this study, the diffraction problem near a circular cylinder and the ship motion problem in oblique waves have been solved using Rankine panel method based on the weak-scatterer hypothesis.

The weak-scatterer assumption provides a part of nonlinearity on the free surface waves. In the diffraction problem, the effect of this nonlinearity on the free surface profile and force signals was observed. Nonlinear waves shorter than the linear waves were observed near the body, and the force signals showed some phase shift and amplitude change. In particular, the second-order effect was dominant in the vertical force.

The weak-scatterer method is more applicable to the ship motion problem. The present study showed a successful simulation of the nonlinear ship motion in oblique waves, and the motion RAOs were very close to the experimental data. In particular, the nonlinearity at RAO peaks has been considered very successfully.

References

DALZELL, J.F., THOMAS III, W.L. AND LEE, W.T. 1992 Correlations of model data with analytical load predictions for three high speed ships. Naval Surface Warfare Center, Ship Hydrodynamics Department Report

HUANG, Y. AND SCLAVOUNOS, P.D. 1998 Nonlinear ship motions. J. of Ship Research, **42, 2**

KIM, Y., KRING, D.C. AND SCLAVOUNOS, P.D. 1997 Linear and nonlinear interactions of surface waves with bodies by a three-dimensional Rankine panel method. Applied Ocean Research, **19**, pp. 235-249

KIM, Y. AND SCLAVOUNOS, P.D. 1999 Numerical Simulation of the linear and second-order surface flows around circular cylinders in random waves. Proc, the 8th Int'l Workshop on Water Waves and Floating Bodies, Port Huron, MI

KIM, Y., KIM, S., RENICK, D. AND SCALVOUNOS, P.D. 1999 Linear and nonlinear flows and responses of ships by a Rankine panel method. Proc, the 7th Int'l Conf on Numerical Ship Hydrodynamics, Nante. France

KRING, D.C. AND SCLAVOUNOS, P.D. 1995 Numerical stability analysis for time-domain ship motion simulation. J. of Ship Research, **39, 4**

LIN, W.M. AND YUE, D.K.P. 1990 Numerical solutions for large-amplitude ship motions in time domain. Proc, the 18th Symp on Naval Hydrodynamics, Ann Arbor. MI

LONGUET HIGGINS, M.D. AND COKELET, E.D. 1976 The deformation of steep surface waves on water I. Proc, Royal Society of London, Series A, **350**, pp. 1-26

NAKOS, D.E. 1990 Ship wave pattern and motions by a three dimensional Rankine panel method. PhD thesis, Department of Ocean Engineering, MIT

NAKOS, D.E. 1993 Stability of transient gravity waves on a discrete free surface. MIT Report

PAWLOWSKI, J. 1992 A nonlinear theory of ship motions in waves. Proc, the 19th Symp on Naval Hydrodynamics, Seoul, Korea

SCLAVOUNOS, P.D. AND NAKOS, D.E. 1988 Stability analysis of panel methods for free-surface flows with forward speed. Proc. the 17th Symp on Naval Hydrodynamics, Hague, The Netherlands